Chemical Engineering Journal 232 (2013) 237–248

Contents lists available at ScienceDirect

Chemical Engineering Journal

journal homepage: www.elsevier.com/locate/cej

Transport of colloids in unsaturated packed columns: Role of ionic strength and sand grain size

Polyxeni N. Mitropoulou [a], Vasiliki I. Syngouna [a], Constantinos V. Chrysikopoulos [b,*]

[a] Department of Civil Engineering, University of Patras, 26500 Patras, Greece
[b] Department of Environmental Engineering, Technical University of Crete, 73100 Chania, Greece

HIGHLIGHTS

- Colloid fate and transport in unsaturated porous media.
- Evaluation of the combined effects of ionic strength and collector size on transport.
- Experimental and theoretical estimation of collision efficiencies.
- Retention of the bigger colloids was slightly higher than smaller colloids.
- Microsphere mass recovery was decreased with increasing ionic strength.

GRAPHICAL ABSTRACT

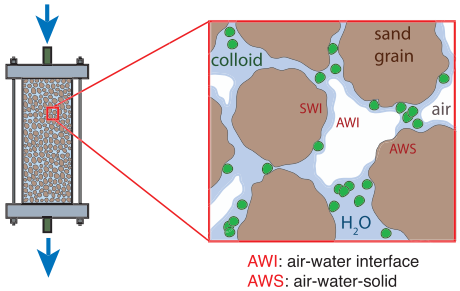

ARTICLE INFO

Article history:
Received 6 May 2013
Received in revised form 20 July 2013
Accepted 23 July 2013
Available online 31 July 2013

Keywords:
Unsaturated porous media
Colloids
Ionic strength
Grain size
Quartz sand
Attachment efficiency

ABSTRACT

The main objective of this study was to better understand the combined effects of ionic strength, and sand grain size on colloid fate and transport in unsaturated porous media. Spherical fluorescent polymer microspheres with three different sizes (0.075, 0.30 and 2.1 μm), and laboratory columns packed with two size fractions of clean quartz sand (0.513 and 0.181 mm) were used. The saturation level of the packed columns was set to 83–95% with solutions having a wide range of ionic strength (0.1–1000 mM). The electrophoretic mobility of colloids and sand grains were evaluated for various ionic strength conditions. The single collector removal and collision efficiencies were quantified using the classical colloid filtration theory. Furthermore, theoretical collision efficiencies were estimated with appropriate DLVO energies using a Maxwell model. The experimental results suggested that the retention of the bigger colloids (2.1 μm) was slightly higher compared to the conservative tracer and smaller colloids (0.3 and 0.075 μm) in deionized-distilled-water, indicating attachment at air–water interfaces or straining. Moreover, relatively smaller attachment was observed onto fine than medium quartz sand. The mass recovery of the 0.3 μm microspheres in NaCl solution was shown to significantly decrease with increasing ionic strength. Both the experimental and theoretical collision efficiencies based on colloid interactions with solid–water interfaces, were increased with increasing ionic strength.

1. Introduction

The transport and fate of colloids and biocolloids in water saturated porous and fractured media has been extensively studied by numerous investigators due to its significant importance in numerous multidisciplinary areas including ground water contamination, subsurface bioremediation, water and wastewater treatment, and artificial aquifer recharge [1–11]. Furthermore, considerable number of theoretical and experimental investigations have focused on various aspects of colloid and biocolloid transport in unsaturated porous media [12–23].

Colloid and biocolloid fate and transport in unsaturated porous media is substantially different than that in saturated porous media. In addition to the retention mechanisms occurring in saturated

* Corresponding author. Tel.: +30 28210 37797; fax: +30 28210 37847.
E-mail address: cvc@enveng.tuc.gr (C.V. Chrysikopoulos).

1385-8947/$ - see front matter © 2013 Elsevier B.V. All rights reserved.
http://dx.doi.org/10.1016/j.cej.2013.07.093

Nomenclature

A_{123}	Hamaker constant, $(ML^2)/t^2$
C	effluent concentration, M/L^3
C_{ss}	effluent concentration at steady state conditions, M/L^3
C_u	sand coefficient of uniformity, –
C_0	infulent concentration, M/L^3
d_c	collector diameter, L
d_p	particle diameter, L
d_{10}	sand grain diameter size that can barely pass through a sieve, which allows 10% of the material (by weight) to pass through, L
d_{60}	sand grain diameter size that can barely pass through a sieve, which allows 60% of the material (by weight) to pass through, L
e	elementary charge, C
E_k	kinetic energy, J
h	particle-collector separation distance, L
i	subscript indicates colloids or tracer, –
I_s	ionic strength, mol/L
k_B	Boltzman's constant, J/K
k_c	deposition rate coefficient, 1/t
L	column length, L
m_n	nth absolute temporal moment, defined in Eq. (1), $t^{n+1}M/L^3$
M_r	mass recovery, defined in Eq. (2)
n	subscript indicating the order of the moment, –
N_A	Avogadro's number, 1/mol
r_p	colloidal particle radius, L
R_p	radius ratio of two colloidal particles, –
S_w	degree of saturation (ratio of volumetric moisture content to porosity), –
T	temperature, K
t_p	injection time period, t
U	interstitial or pore water velocity, L/t
w_f	film thickness, L
x	spatial coordinate in the horizontal direction, L
Z	ionic charge, –

Greek letters

α	collision efficiency, –
α_{exp}	experimental collision efficiency, –
α_{th}	theoretical collision efficiency, –
ε	dielectric constant of the suspending liquid, C^2t^2/ML^2
ε_r	relative dielectric constant of the suspending liquid, –
ε_0	permittivity of free space, C^2t^2/ML^2
ζ	electrokinetic zeta potential, V
η_0	single-collector removal efficiency for favorable deposition, –
η_{exp}	experimental single-collector removal efficiency –
θ	porosity (voids volume to porous medium volume), L^3/L^3
θ_m	moisture content or volumetric water content (liquid volume to porous medium volume), L^3/L^3
κ	Debye–Huckel parameter, 1/L
λ	characteristic wavelength of the sphere–plate or sphere–sphere interaction, L
ρ_p	colloidal particle density, M/L^3
σ_{aw}	air–water surface tension, M/t^2
σ_{Born}	Born collision parameter, L
Φ_{Born}	Born potential energy, ML^2/t^2
Φ_{DLVO}	DLVO potential energy, ML^2/t^2
Φ_{dl}	double layer potential energy, ML^2/t^2
Φ_{max1}	primary maximum of Φ_{tot}, ML^2/t^2
Φ_{min1}	primary minimum of Φ_{tot}, ML^2/t^2
Φ_{min2}	secondary minimum of Φ_{tot}, ML^2/t^2
Φ_{vdW}	van der Waals potential energy, ML^2/t^2
ψ	matric potential, M/Lt^2
ψ_c	critical matric potential, M/Lt^2
Ψ_c	surface potential of the collector (sand), V
Ψ_p	surface potential of the colloid particle, V

Abbreviations

AWI	air–water interface
AWS	air–water–solid
CFT	colloid filtration theory
DLVO	Derjaguin–Landau–Verwey–Overbeek
ddH_2O	deionized distilled water
SWI	solid–water interface

porous media (e.g., pore straining, and attachment onto solid–water interfaces (SWI)), the presence of a gaseous phase in unsaturated porous media creates other potential retention sites associated with air–water interfaces (AWI), and air–water–solid (AWS) surfaces [12,20,24–26]. The AWS surface is essentially the area where air, water and solid grain approach each other to a triple contact. Furthermore, in unsaturated porous media colloids and biocolloids can also be retained in thin water films (film straining) that envelop solid grains [14,27]. A schematic illustration of the various interfaces encountered in unsaturated porous media as well as the attachment and colloid retention possibilities during colloid transport is shown in Fig. 1.

Despite these and other related research efforts, our understanding of the specific interactions between colloids and SWI, AWI and AWS that exist in unsaturated porous media are somewhat limited. Also, the extent to which retention is influenced by physicochemical changes in an unsaturated system (i.e., collector size, degree of saturation) remains poorly understood.

Ionic strength and grain size are known to impact colloid transport in porous media; however, to our knowledge, their combined effects on colloid transport and retention in unsaturated porous media has not been previously explored. To fill the knowledge

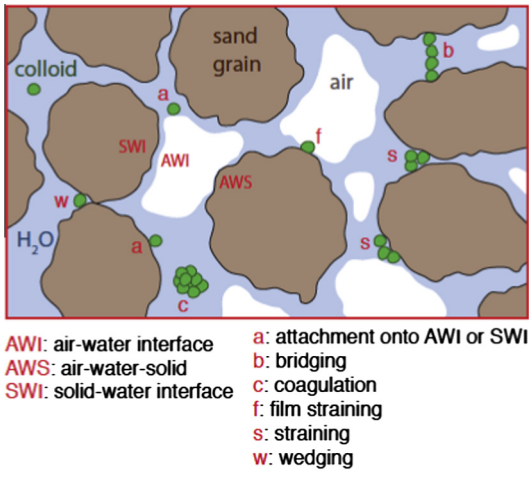

Fig. 1. Schematic illustration of colloid particle attachment and straining during transport in unsaturated porous media.

gap, our objective was to investigate how various combinations of ionic strength values and grain sizes can impact the transport and retention of colloids in laboratory-scale unsaturated sand columns. The collision efficiencies of the three colloids examined were estimated experimentally and theoretically, and the various factors that control colloid deposition were discussed.

2. Materials and experimental procedures

2.1. Colloids

Spherical fluorescent polystyrene microspheres (Duke Scientific Corp., Palo Alto, CA) of three different sizes (0.075, 0.30 and 2.1 μm in diameter) with density of 1.05 g/cm^3 and a refractive index of 1.59 were used in this study as ideal colloids. The excitation and emission wavelengths of the three selected microspheres are: 468 nm and 508 nm for the 0.075 μm (green) microspheres, 542 nm and 612 nm for the 0.30 μm (red) microspheres, and 364 nm and 447 nm for the 2.1 μm (blue) microspheres, respectively. Prior to each experiment, the microsphere stock suspensions were diluted in deionized distilled water (ddH_2O), which was purified to a specific conductance of 17.8 μS/cm with water from a Milli-Q UV plus purification system (Millipore Corp., MA) containing a filter with 0.22 μm pore size and UV sterilization. The initial concentrations of the red, green and blue microsphere stock suspensions were 6.74×10^{11}, 4.31×10^{13}, and 1.96×10^{9} N_c/mL, respectively, where N_c denotes number of colloids.

For the experiments with influent colloid solutions having different ionic strength, only the green (0.075 μm) and red (0.30 μm) microspheres were employed. The green microspheres stock suspension was diluted in 0.1–10 mM NaCl solutions by a factor of 10^4 so that the initial concentration was set to $C_0 = 4.31 \times 10^8$ N_c/mL, and the red microspheres stock suspension was diluted in 0.1–1000 mM NaCl solutions by a factor of 500 to $C_0 = 1.35 \times 10^8$ N_c/mL. Note that although influent colloids were suspended in NaCl solutions, background influent solutions were free of NaCl. All effluent microsphere concentrations were measured by fluorescence spectrophotometer (Cary Eclipse, Varian, Inc.). Each effluent colloid concentration was measured three times, and each experiment was repeated at least three times. Note that each concentration measurement required only 0.3 mL of effluent sample, and all sample analyses were carried out immediately after the completion of each experiment.

2.2. Porous media

Two types of quartz sand (Filcom, Filterzand and Grind) were used to pack the columns: (1) "medium" sand with a mean grain diameter of 0.513 mm (Sieve No 40: 0.425–0.600 mm), and (2) "fine" sand with a mean grain diameter of 0.181 mm (sieve no 100: 0.150–0.212 mm). Particle size distribution values obtained by sieve analysis were used to estimate the coefficient of uniformity ($C_u = d_{60}/d_{10}$, where d_{10} and d_{60} is the diameter of a sand grain that is barely too large to pass through a sieve that allows 10% and 60%, respectively, of the material by weight to pass through). It was determined that $C_u = 1.21$, 1.19 for medium and fine sand, respectively. The chemical composition of the sand reported by the manufacturer was: 96.2% SiO_2, 0.15% Na_2O, 0.11% CaO, 0.02% MgO, 1.75% Al_2O_3, 0.78% K_2O, 0.06% SO_3 and 0.46% Fe_2O_3, 0.03% P_2O_5, 0.02% BaO, and 0.01% Mn_3O_4. The total organic carbon content was measured by the Walkley–Black method (i.e., chemical oxidation of the organic fraction) and was found equal to 0.1 ± 0.1% for both medium and fine sand fractions [28]. The sands were thoroughly washed using the procedures outlined by Syngouna and Chrysikopoulos [29]. Briefly, sand washing included soaking in concentrated 0.1 M HNO_3 (70%), and sonication to remove organic matter. After the cleaning steps, the sand was dried in an oven at 105 °C and then stored in screw cap sterile beakers until use in the column experiments.

2.3. Electrokinetic measurements

The zeta potential, ζ, of the various colloids and sands used in this study was measured in solutions with different ionic strength by a zetasizer (Nano-ZS90, Malvern Instruments, Southborough, MA). Note that sand grains were too large for direct measurement of their zeta potential by the zetasizer. Therefore, a few sand grains were crushed into fine powder and then mixed with the appropriate solution of each ionic strength to form a sufficiently stable suspension that could be used for zeta potential measurement [30]. All zeta potential measurements were obtained in triplicates and the values are shown in Table 1. These zeta potentials were used to calculate the required electrostatic interaction energies between colloids and SWIs. Furthermore, the electrostatic interactions between colloids and AWIs were calculated using the following previously reported zeta potentials for air bubbles present in unsaturated packed columns under various conditions: ζ = −65 mV in 0.1 mM NaCl solution [15,31], and ζ = −25.8, −20.4, and −13.6 mV in 1, 10, and 100 mM NaCl solutions, respectively [32].

2.4. Transport experiments

Colloid transport experiments were conducted in a Plexiglas© column with length 15.2 cm and internal diameter 2.61 cm. The experimental setup is similar to that described in detail by Anders and Chrysikopoulos [22]. Briefly, the column was uniformly wet-packed with quartz sand. Several pore volumes of the de-aired background solution were passed through the column from the bottom at a rate of 1 mL/min to avoid the capture of air bubbles. The porosity, the average water saturation level, and the bulk density of the packed column were determined gravimetrically. The packed column was attached to a vacuum chamber (Soil Measurement Systems, Tucson, AZ) with a fraction collector inside, as shown in Fig. 2, which allowed for various levels of water saturation. The packed column was placed above the vacuum chamber with its lower outlet connected to the vacuum chamber. The colloid suspension was applied using a syringe pump in order to set the injection rates necessary in order to maintain a steady water potential for the duration of the experiment. The water potential and the uniformity of water in the column were verified with tensiometer readings taken at two locations (2.5 and 7.5 cm from the upper sand surface), which were collected continuously using a CR800 datalogger (Campbell Scientific, Inc., Logan, UT). Note that for each colloid transport experiment the saturated column was drained to the desired water saturation level by reducing the inflow water rate to the hydraulic conductivity corresponding to that saturation. Simultaneously, the pressure head at the bottom of the column was gradually reduced until the readings of the tensiometers showed exactly the same

Table 1
Zeta potentials of quartz sand and microspheres for various ionic strengths.

I_s (mM)	ζ (mV)			
	Microspheres		Quartz sand	
	Green (d_p = 0.075 μm)	Red (d_p = 0.3 μm)	Medium	Fine
0.1	−27.3 ± 4.2	−48.9 ± 9.8	−55.47 ± 1.3	−62.55 ± 3.0
1	−30.7 ± 1.2	−43.5 ± 8.1	−54.9 ± 1.8	−62.6 ± 2.3
10	−23.5 ± 3.5	−75.46 ± 3.1	−50.07 ± 3.0	−57.02 ± 1.7
100	−26.97 ± 1.9	−35.45 ± 1.6	−19.8 ± 1.3	−20.47 ± 0.6

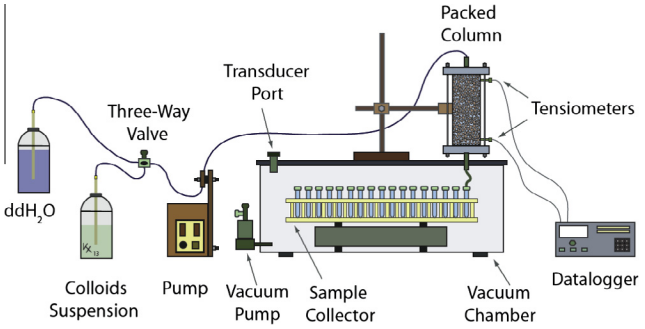

Fig. 2. Schematic illustration of the experimental apparatus.

values. This resulted in a constant capillary pressure, which implies a constant saturation level along the column. The experimental conditions of each column experiment are listed in Table 2. Liquid samples were collected at regular time intervals from the column effluent in small fractions with an automatic fraction collector. The pressure inside the vacuum chamber was controlled by the pressure regulator and monitored by a tensiometer attached to the tensiometer port.

The mean pH of the column influent remained constant during each experiment at 7.0 ± 0.2. For each of the two sand grain sizes selected, transport experiments were run using a tracer and three different colloid solutions with a wide range of ionic strength (I_s = 0.1–1000 mM). Chloride, in the form of 10 mM sodium chloride (NaCl), was chosen as the nonreactive tracer. It should be noted that alkali halides are the most commonly used salts for subsurface fluid tracing [33]. All effluent chloride concentrations were measured using ion chromatography (ICS-1500, Dionex Corp., Sunnyvale, CA).

3. Theoretical considerations

3.1. Moment analysis

The colloid concentration breakthrough data obtained at the end of the packed column ($x = L$) were analyzed by the absolute temporal moments [34]:

$$m_n(x) = \int_0^\infty t^n C_i(x,t)dt \tag{1}$$

where the subscript n = 0, 1, 2, … indicates the order of the moment, t is time, C [M/L^3] is the effluent concentration, and subscript i indicates colloids or tracer. The zeroth absolute temporal moment, m_0 [tM/L^3], quantifies the total mass in the concentration breakthrough curve; the first absolute moment, m_1 [t^{2}M/L^3], describes the mean residence time; and second absolute temporal moment, m_2 [t^{3}M/L^3], describes the degree of spreading of the concentration breakthrough curve. Furthermore, the mass recovery, M_r [−], of the tracer or the suspended particles is quantified by the following expression:

$$M_r(L) = \frac{m_0(L)}{C_{i_0} t_p} = \frac{\int_0^\infty C_i(L,t)dt}{\int_0^{t_p} C_i(0,t)dt} \tag{2}$$

where L is the column length, and t_p is the duration of the solute pulse.

3.2. Filtration theory

The classical colloid filtration theory (CFT) was used to quantitatively compare the attachment of colloids onto quartz sand. The CFT is employed for the estimation of the dimensionless collision efficiency, α, which represents the ratio of the collisions resulting in attachment to the total number of collisions between particles and collector grains [35]. Column experiments in "clean-beds" (α = 1) are commonly used to empirically determine α for a given set of physicochemical conditions. Following the work by Saiers and Lenhart [36], the collision efficiencies for unsaturated transport experiments were estimated using the CFT relationship by adjusting for the reduced water content compared to saturated porous media by multiplying the porosity, θ [−], with the degree of saturation, $S_w = \theta_m/\theta$ (where θ_m [−] is the moisture content or volumetric water content defined as the ratio of the liquid volume to the porous medium volume):

$$\alpha = k_c \frac{2d_c}{3U} \frac{\theta S_w}{(1-\theta S_w)\eta_0} = k_c \frac{2d_c}{3U} \frac{\theta_m}{(1-\theta_m)\eta_0} \tag{3}$$

where k_c [1/t] is the deposition rate coefficient, d_c [L] is the mean collector diameter, U [L/t] is the interstitial water velocity, and η_o is the single-collector contact efficiency, which can be calculated

Table 2
Experimental conditions and estimated parameters.

Experiments	Colloid d_p (μm)	Quartz sand	I_s (mM)	θ_m (−)	S_w (−)	U (cm/min)	M_r (%)	α_{exp} (−)
1	0.075	Fine	ddH$_2$O	0.36	0.91	0.71	94.4	0.0010
2	0.075	Medium	ddH$_2$O	0.39	0.86	0.64	91.3	0.0055
3	0.3	Fine	ddH$_2$O	0.34	0.95	0.52	100	0.0000
4	0.3	Medium	ddH$_2$O	0.34	0.86	0.71	100	0.0002
5	2.1	Fine	ddH$_2$O	0.36	0.86	0.69	91.3	0.0057
6	2.1	Medium	ddH$_2$O	0.39	0.93	0.67	90.6	0.0555
7	0.075	Fine	1	0.26	0.85	0.9	73.6	0.0021
8	0.075	Fine	5	0.24	0.78	0.93	40.4	0.0050
9	0.075	Medium	0.1	0.34	0.85	0.71	98.1	0.0010
10	0.075	Medium	1	0.33	0.92	0.78	95.6	0.0024
11	0.075	Medium	5	0.37	0.91	0.69	46.4	0.0467
12	0.075	Medium	10	0.32	0.79	0.7	30.1	0.0500
13	0.3	Fine	1	0.32	0.9	0.79	78.5	0.0065
14	0.3	Fine	5	0.22	0.79	1	43.8	0.0125
15	0.3	Medium	0.1	0.31	0.85	0.78	100	0.0000
16	0.3	Medium	1	0.32	0.9	0.79	79.7	0.0339
17	0.3	Medium	5	0.32	0.87	0.78	24.8	0.1990
18	0.3	Medium	50	0.39	0.91	0.66	37.2	0.1930
19	0.3	Medium	100	0.34	0.81	0.68	45.8	0.1080
20	0.3	Medium	1000	0.39	0.91	0.66	5.2	0.5770
21	Tracer	Fine	10	0.42	0.85	0.57	100	–
22	Tracer	Medium	10	0.22	0.47	0.59	100	–

from the relationship proposed by Tufenkji and Elimelech [37] by replacing θ with θ_m.

Note that k_c for unsaturated conditions can be obtained from familiar expressions developed for saturated conditions [38] with appropriate modifications to account for the reduced water content:

$$k_c = \frac{3}{2}\frac{(1-\theta_m)^{1/3}U}{d_c\theta_m}\eta_{exp} \quad (4)$$

where η_{exp} [−] is the experimental single-collector efficiency evaluated by the following expression:

$$\eta_{exp} = -\frac{2}{3}\frac{d_c}{L(1-\theta_m)^{1/3}}\ln\left[\frac{C_{ss}}{C_0}\right] \quad (5)$$

where C_0 [M/L^3] is the influent colloid concentration, and C_{ss} [M/L^3] is the effluent colloid concentration after the breakthrough curve has reached steady state conditions. Combining Eqs. (3)–(5) yields the desired expression for the experimental collision efficiency, α_{exp}, in unsaturated packed columns:

$$\alpha_{exp} = -\frac{2}{3}\frac{d_c}{L(1-\theta_m)\eta_0}\ln\left[\frac{C_{ss}}{C_0}\right] \quad (6)$$

3.3. DLVO interaction energy calculations

Colloid retention greatly depends on the total DLVO interaction energy. To better understand the observed colloid transport and deposition behavior in the unsaturated column experiments conducted in this study, the interaction energy between two colloids as well as colloid–SWI or colloid–AWI were calculated. The total interaction energy Φ_{DLVO} [J] between two surfaces is determined as a function of the separation distance h [m] by the expression [39]:

$$\Phi_{DLVO}(h) = \Phi_{vdW}(h) + \Phi_{dl}(h) + \Phi_{Born}(h) \quad (7)$$

where Φ_{vdW} [J] is the van der Waals interaction energy, Φ_{dl} [J] is the electrostatic interaction energy, and Φ_{Born} [J] is the Born interaction energy. Note that the DLVO interaction energies are estimated by assuming that the colloid–colloid, and colloid–sand or colloid–air systems can be represented by the ideal sphere–sphere, and sphere–plate models, respectively.

The Φ_{vdW} interaction energy between two spheres in water (i.e., colloid to colloid) is evaluated by [40,41]:

$$\Phi_{vdW}(h) = -\frac{A_{121}}{12}\left\{\frac{R_p}{\xi^2+\xi R_p+\xi} + \frac{R_p}{\xi^2+\xi R_p+\xi+R_p} + 2\ln\left[\frac{\xi^2+\xi R_p+\xi}{\xi^2+\xi R_p+\xi+R_p}\right]\right\} \quad (8)$$

where

$$R_p = \frac{r_{p2}}{r_{p1}} \quad (9)$$

$$\xi = \frac{h}{r_{p1}} \quad (10)$$

r_{p1} [m] is the radius of the spherical colloid particle 1, and r_{p2} [m] is the radius of the spherical colloid particle 2 (usually $r_{p1} \leqslant r_{p2}$). In this study $R_p = 1$ because the spheres (colloids) are identical ($r_{p1} = r_{p2}$). For the sphere to plate interactions, the Φ_{vdW} interaction is determined by [42]:

$$\Phi_{vdW}(h) = -\frac{A_{123}r_p}{6h}\left[1+\left(\frac{14h}{\lambda}\right)\right]^{-1} \quad (11)$$

where A_{123} [J] is the combined Hamaker constant for microscopic bodies of composition "1" and "3" in medium "2" [(1-colloid)-(2-water)-(3-solid/air)], $\lambda \sim 10^{-7}$ m is the characteristic wavelength of the sphere–plate or sphere–sphere interactions, and r_p [m] is the colloid particle radius. The Hamaker constant values were taken from the literature: $A_{cwc} = 1.3\times10^{-20}$ J for the colloid–water–colloid interaction [23], $A_{cws} = 6.5\times10^{-21}$ J for the colloid–water–sand interaction, and $A_{cwa} = -1.05\times10^{-20}$ J for the colloid–water–air interaction [15]. These Hamaker constants imply that van der Waals interactions are attractive when colloids approach a SWI and repulsive when colloids reach an AWI.

Assuming that the surface potentials are constant, the Φ_{dl} between two colloids is given by [43]:

$$\Phi_{dl}(h) = \pi\varepsilon_r\varepsilon_0 \times \frac{r_{p1}r_{p2}}{(r_{p1}+r_{p2})}\left[2\Psi_{p1}\Psi_{p2}\ln\left(\frac{1+e^{-\kappa h}}{1-e^{-\kappa h}}\right) + (\Psi_{p1}^2+\Psi_{p2}^2)\ln(1-e^{-2\kappa h})\right] \quad (12)$$

Note that in this study $r_{p1} = r_{p2}$. Furthermore, the Φ_{dl} between a colloid and SWI or AWI can be calculated by the following expression [43]:

$$\Phi_{dl}(h) = \pi\varepsilon_r\varepsilon_0 r_p\left[2\Psi_p\Psi_c\ln\left(\frac{1+e^{-\kappa h}}{1-e^{-\kappa h}}\right) + (\Psi_p^2+\Psi_c^2)ln(1-e^{-2\kappa h})\right] \quad (13)$$

where $\varepsilon_r = \varepsilon/\varepsilon_0$ [−] is the dimensionless relative dielectric constant of the suspending liquid, ε [C^2/(J m)] is the dielectric constant of the suspending liquid, ε_0 [C^2/(J m)] is the permittivity of free space, Ψ_p [V] is the surface potential of the colloid particle, Ψ_c [V] is the surface potential of the collector surface SWI or AWI (plate), and κ [1/m] is the inverse of the diffuse layer thickness, known as the Debye–Huckel parameter [44]:

$$\kappa = \left[\frac{2I_sN_A1000e^2}{\varepsilon_r\varepsilon_0k_BT}\right]^{1/2} \quad (14)$$

where I_s [mol/L] is the ionic strength, $N_A = 6.02\times10^{23}$ [1/mol] is Avogadro's number, $e = 1.602\times10^{-19}$ [C] is the elementary charge, $k_B = 1.38\times10^{-23}$ [J/K] is the Boltzmann constant, and $T = 298$ [K] is the fluid absolute temperature. Note that the measured ζ-potentials listed in Table 1 were used in place of the surface potentials.

The Born repulsion is of short-range and results from the overlap of the electron clouds of atoms. The Φ_{Born} between two spheres evaluated by [40,41]:

$$\Phi_{Born}(h) = \frac{A_{123}}{7560\xi}\left(\frac{\sigma_{Born}}{r_{p1}}\right)^2\left[\frac{-4\xi^2-14(R_p-1)\xi-6(R_p^2-7R_p+1)}{(2\xi-1+R_p)^7} + \frac{-4\xi^2+14(R_p-1)\xi-6(R_p^2-7R_p+1)}{(2\xi+1-R_p)^7} + \frac{4\xi^2+14(R_p-1)\xi+6(R_p^2+7R_p+1)}{(2\xi+1+R_p)^7} + \frac{4\xi^2-14(R_p-1)\xi+6(R_p^2+7R_p+1)}{(2\xi-1-R_p)^7}\right] \quad (15)$$

Also, the Φ_{Born} for sphere–plate was estimated by the relationship [44]:

$$\Phi_{Born}(h) = \frac{A_{123}\sigma_{Born}^6}{7560}\left[\frac{8r_p+h}{(2r_p+h)^7} + \frac{6r_p-h}{h^7}\right] \quad (16)$$

where σ_{Born} [m] is the Born collision parameter and usually is taken as $\sigma_{Born} = 5$ Å [44].

The theoretical collision efficiency, α_{th}, is calculated with a Maxwell model, which considers that colloids can be deposited in the secondary minimum or shallow energy "well", Φ_{min2}, as well

as in the primary minimum or deep energy "well", Φ_{min1}, assuming that the colloids possess larger kinematic energy than the total energy barrier, $\Phi_{max1} - \Phi_{min2}$ (where Φ_{max1} is the primary maximum or energy barrier to attachment and detachment) [45]:

$$\begin{aligned}\alpha_{th} &= \alpha_{th(min1)} + \alpha_{th(min2)} \\ &= \int_{\Phi_{max1}-\Phi_{min2}}^{\infty} f(E_k)dE_k + \int_{0}^{-\Phi_{min2}} f(E_k)dE_k \\ &= 1 - \int_{-\Phi_{min2}}^{\Phi_{max1}-\Phi_{min2}} f(E_k)dE_k \end{aligned} \quad (17)$$

where E_k [J] is the kinetic energy of a colloid, and $f(E_k)$ is the Maxwell–Boltzmann distribution function is just a transformation of the Maxwell speed distribution function that describes how particles are distributed in regard to their kinetic energies [46]:

$$f(E_k)dE_k = 2\left[\frac{E_k}{\pi(k_BT)^3}\right]^{1/2} \exp\left[-\frac{E_k}{k_BT}\right]dE_k \quad (18)$$

3.4. Estimation of water film thicknesses

In unsaturated porous media, water is retained by capillarity in the form of pendular rings, and by adsorption in the form of thin films on the solid grain surfaces. If the thickness of an adsorbed water film, w_f [L], is smaller than d_p, film straining occurs. Wan and Tokunaga [14] developed the following expression for the prediction of the thickness of a water film adsorbed onto spherical grains away from pendular ring regions:

$$w_f = \left(\frac{\varepsilon_r\varepsilon_o}{2}\right)^{1/2}\left(\frac{\pi k_BT}{Ze}\right)\left(\frac{4\sigma_{aw}}{d_c} - \psi\right)^{-1/2} \quad (19)$$

where Z [–] is the ionic charge, σ_{aw} [N/m] is the air–water surface tension, and ψ [Pa] is the matric potential that represents the saturation-dependent component of the chemical potential of water. For critical saturation conditions (when pendular rings become discontinuous) and for a close packing (rhombohedral) of uniform spherical grains with diameter d_c, the critical matric potential is given by [14]:

$$\psi_c = -\frac{9.068\sigma_{wa}}{d_c} \quad (20)$$

Note that although wettability alterations in unsaturated porous media can be explained by thin-film stability on the pore surface, colloid migration was reported to play an insignificant role [47].

4. Results and discussion

4.1. Effect of colloid and grain size on colloid transport

Normalized chloride breakthrough data collected from two representative unsaturated experiments with both medium and fine sands using 10 mM NaCl solution are shown in Fig. 3. Note that the breakthrough curves exhibited small concentration fluctuations, presumably due to experimental errors associated with tracer concentration measurements and small variations in water flux. Furthermore, the differences in the two representative tracer breakthrough curves (experiments 21 and 22 in Table 2) shown in Fig. 3 are attributed to the porosity, degree of water saturation, and interstitial velocity differences in the two columns. It is intuitive that faster breakthrough would occur in the medium sand column where the degree of saturation was smaller and the interstitial velocity was higher. The corresponding M_r values were calculated using Eq. (2) and are listed in Table 2. Note that M_r of the tracer was 100% for both medium and fine sands.

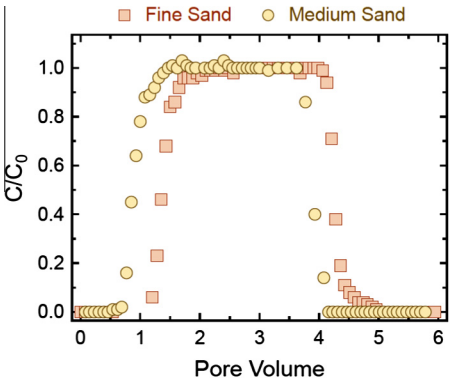

Fig. 3. Tracer breakthrough data for unsaturated columns packed with: (a) fine sand (squares, experiment 21 with $\theta_m = 0.42$, $S_w = 0.85$, and $U = 0.57$ cm/min), and (b) medium sand (circles, experiment 22 with $\theta_m = 0.22$, $S_w = 0.47$, and $U = 0.59$ cm/min).

The normalized breakthrough data of the three microspheres with diameters $d_p = 0.075$, 0.30 and 2.1 μm in ddH_2O, for both quartz sands (medium and fine) are presented in Fig. 4. It should also be noted that the M_r values, listed in Table 2, were calculated using Eq. (2) and indicate that the retention of the blue microspheres (larger colloids with $d_p = 2.1$ μm) was slightly higher than that of the red and green microspheres (smaller colloids with $d_p = 0.30$, and 0.075 μm, respectively). Unlike colloid transport in water saturated porous media where, due to size exclusion, colloid breakthrough concentrations are strongly dependent on particle size [48], the results of Fig. 4 suggest that breakthrough concentrations are affected by the size of the sand, colloid size, as well as the degree of saturation, which controls the water film thickness that leads to film straining.

The blue microspheres are more sensitive to removal mechanisms such as straining (particle trapping in pore throats that are

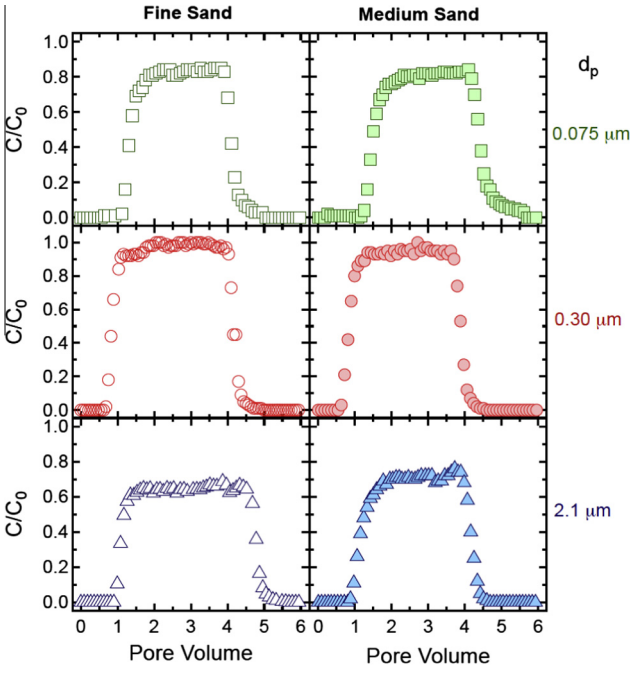

Fig. 4. Experimental breakthrough data for green microspheres with $d_p = 0.075$ μm (squares, experiments 1 and 2), red microspheres with $d_p = 0.3$ μm (circles, experiments 3 and 4), and blue microspheres with $d_p = 2.1$ μm (triangles, experiments 5 and 6) in unsaturated columns packed with fine sand (open symbols), and medium sand (filled symbols). (For interpretation of the references to color in this figure legend, the reader is referred to the web version of this article.)

too small to allow particle passage), film straining (physical restriction of particles in water films which are thinner than d_p), and wedging (particle attachment onto surfaces of two or more collector grains in contact) than the red and green microspheres. It should be noted that the large size of blue microspheres results in colloid to collector diameter ratios (d_p/d_c), which are well above the suggested threshold of 0.004 [49] or 0.003 [50]. The film thicknesses, as predicted by Eq. (19) for 1:1 NaCl solution at 25 °C and near-critical saturations with $\sigma_{aw} = 0.0718$ N/m, are equal to $w_f = 21$ nm for the fine sand ($d_c = 0.181$ mm), and $w_f = 36$ nm for the medium sand ($d_c = 0.513$ mm). These w_f values are considerably thinner than the diameters of the colloids used in this study ($d_p = 0.075$, 0.30 and 2.1 μm). Under these conditions ($w_f < d_p$), film straining is important, because strong capillary forces can pin colloids to the solid surfaces and/or colloids can get trapped in pendular ring regions, which are separated from the remaining fluids by thin water films [14]. When the water films expand, these trapped colloids can be remobilized [25]. Note that colloids have been observed to immobilize at or near AWS interfaces [17,24].

The blue microspheres ($d_p = 2.1$ μm) and green microspheres ($d_p = 0.075$ μm) were retained slightly more by the medium than fine sand under ddH_2O conditions (see Table 2). The calculated average volumetric water content for the fine sand was $\theta_m = 0.32 \pm 0.07$, and for the medium sand $\theta_m = 0.34 \pm 0.05$. Grain surface irregularities and roughness may have played an important role in influencing colloid retention in the form of clusters (non-uniformly distributed) on the grain surfaces [51]. For the fine sand case, the small pore volume may have increased the possibility for microspheres to be filtered-out [52]. Although colloid collision efficiency increases with increasing collector diameter, CFT theory still predicts greater attachment for smaller collectors [29,53]. During flow of colloid suspensions through porous media, colloid particles are gradually retained by solid matrix causing pore space geometry alterations, permeability reduction, and in turn, colloid deposition changes [54]. In this study the duration of the experiments was relatively short, and the colloid concentrations used were low. Therefore, particle deposition was not expected to significantly alter the collector surfaces. However for longer injection periods or when higher colloid concentrations are used, the deposition rates are expected to be time dependent.

4.2. Effect of ionic strength on colloid transport

The data from the transport experiments conducted using red microspheres ($d_p = 0.3$ μm), a column packed with medium quartz sand, and influent solutions with various ionic strengths ($I_s = 0.1$, 1, 5, 50, 100, and 1000 mM NaCl) are presented in Fig. 5. Clearly, the deposition of the red microspheres ($d_p = 0.3$ μm) exhibited a very strong dependence on I_s (see Fig. 5), with M_r values ranging between 5% and 100%. Note that at low ionic strength ($I_s = 0.1$ mM) the microspheres did not attach onto the sand surfaces. This observation is consistent with the DLVO theory, suggesting that the energy barriers were very high and the secondary energy minima were too small to allow either primary or secondary energy minima deposition. Thus, incomplete breakthrough of colloids is an indication of physical straining [55]. If the ionic strength increases, colloids loosely retained within secondary energy minimum can be subjected to flow drag and translate down gradient [56]. Furthermore, Fig. 6 presents the normalized breakthrough data from transport experiments using the green ($d_p = 0.075$ μm) and red ($d_p = 0.3$ μm) microspheres in unsaturated columns packed with fine and medium quartz sand for influent solutions with $I_s = 1$, and 5 mM. The M_r values were computed for each experiment, and the results are listed in Table 2. As the ionic strength increased from $I_s = 1$ mM to $I_s = 5$ mM, physicochemical filtration was probably the dominant mechanism of colloid filtration. Significant

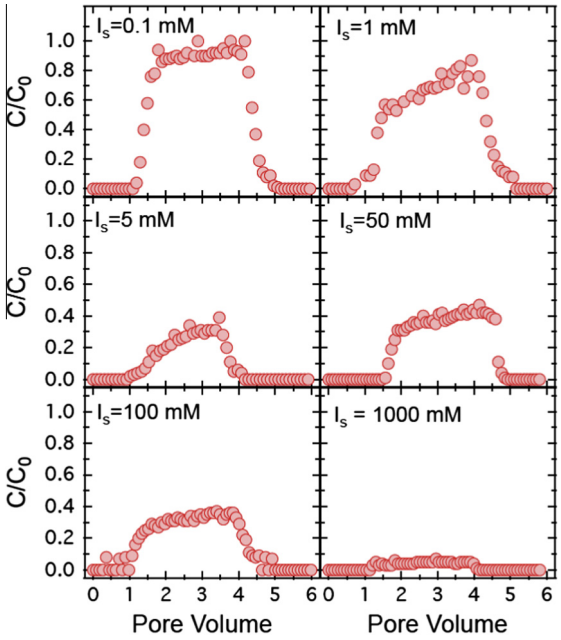

Fig. 5. Experimental breakthrough data for red microspheres ($d_p = 0.3$ μm) in unsaturated columns packed with medium sand for influent solutions having different ionic strengths (experiments 15–20).

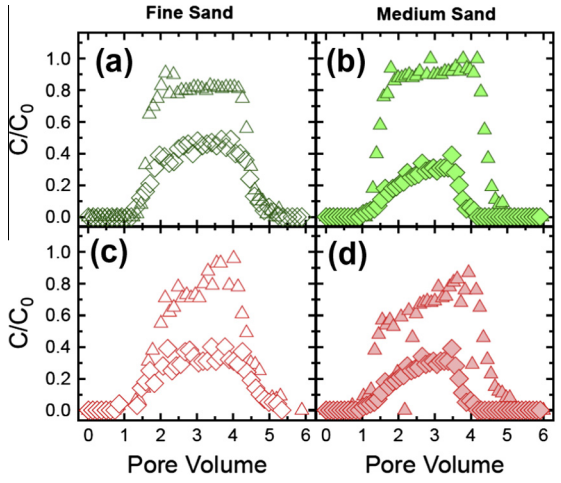

Fig. 6. Experimental breakthrough data for: (a) and (b) green microspheres ($d_p = 0.075$ μm), and (c) and (d) red microspheres ($d_p = 0.3$ μm) in unsaturated columns packed with fine sand (open symbols), and medium sand (filled symbols). The data for $I_s = 1$ mM are represented with triangles, and for $I_s = 5$ mM with diamonds ((a) experiments 7 and 8, (b) experiments 10 and 11, (c) experiments 13 and 14, and (d) experiments 16 and 17).

colloid retention was observed at $I_s = 5$ mM. Note that only 40.4–46.4% of the green microspheres ($d_p = 0.075$ μm) and 24.8–43.8% of the red microspheres ($d_p = 0.3$ μm) passed through the column at $I_s = 5$ mM (see Table 2). The M_r values as a function of I_s and d_p reported in Table 2 are also graphically illustrated in Fig. 7.

4.3. Collision efficiencies

Fig. 8 presents the experimental collision efficiencies, α_{exp}, for the green ($d_p = 0.075$ μm) and red microspheres ($d_p = 0.3$ μm), as predicted by Eq. (6) using the parameter values listed in Table 2.

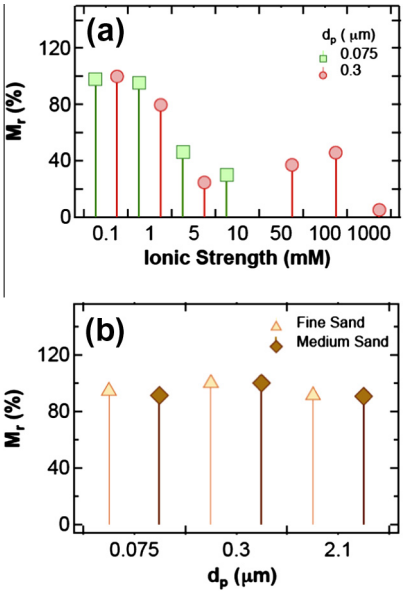

Fig. 7. Estimated M_r values for (a) green and red microspheres as a function of I_s, and (b) fine and medium sand as a function of d_p.

The calculated α_{exp} values varied by several orders of magnitude because they depend on a variety of parameters, including the nature of the grain surface [57], solution I_s [58], presence of natural organic matter [59], and colloid surface properties [60]. The calculated α_{exp} values indicate that more favorable attachment conditions existed for the red microspheres (d_p = 0.3 μm) than for the green microspheres (d_p = 0.075 μm). In a similar study, Hahn et al. [61] used latex microspheres and observed that α_{exp} was higher for the larger colloids than the smaller ones, and emphasized the dominance of secondary minimum deposition on colloid retention in porous media. The experimental data from this study suggest that α_{exp} values increase with increasing I_s. Also, Fig. 8 shows that there is a strong dependence of α_{exp} on d_c, suggesting that greater amounts of colloids are attached onto larger than smaller sand grains. This observation is in agreement with the works by Torkzaban et al. [53] and Syngouna and Chrysikopoulos [29] who have suggested that the drag force acting on the colloids along the collector surface decreases with increasing collector size. Worthy to note is that contradictory observations of smaller collectors associated with greater amounts of colloid retention have also been reported in the literature [62]. According to CFT the deposition profile is expected to be independent of the colloid and grain size. However in the presence of an energy barrier to deposition, colloid deposition efficiencies, as a function of colloid size, cannot be expected to follow the trend predicted by CFT [63]. Moreover, small variations in colloid surface properties (e.g. in the colloid surface charge) [64,65] could yield sufficient variations in the attachment coefficient to produce hyper-exponential deposition profiles. Deviations between CFT and experimental deposition profiles have been reported to increase with increasing I_s and d_p and decreasing d_c [18]. Note that all of these observations suggest that attachment (in Φ_{min1} or Φ_{min2} of DLVO potential energy distribution) is not the only factor controlling deposition.

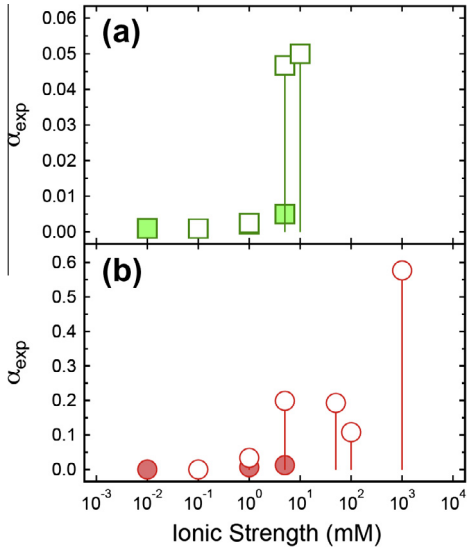

Fig. 8. Experimental collision efficiencies in unsaturated columns packed with fine sand (filled symbols) and medium sand (open symbols) as a function of ionic strength for: (a) green microspheres (d_p = 0.075 μm), and (b) red microspheres (d_p = 0.3 μm).

4.4. DLVO energy profiles

The total Φ_{DLVO} interaction energy, according to the DLVO theory, for the experimental conditions of this study (pH = 7, I_s = 0.1, 1, 10 and 100 mM) are presented for colloid–colloid (sphere–sphere) interactions in Fig. 9, colloid–SWI (sphere–plate) interactions in Fig. 10, and colloid–AWI (sphere–plate) interactions in Fig. 11. Also, the estimated Φ_{min1}, Φ_{min2} and Φ_{max1} values of the DLVO energy curves are listed in Table 3.

The DLVO energy profiles in Figs. 9 and 10 indicate that a negative Φ_{min1} does not exist for colloid–SWI and colloid–colloid interactions under the experimental conditions of this study (pH = 7, I_s = 0.1, 1, 10 and 100 mM), except the case of green microspheres (d_p = 0.075 μm) and fine sand at I_s = 0.1 mM (see Table 3).

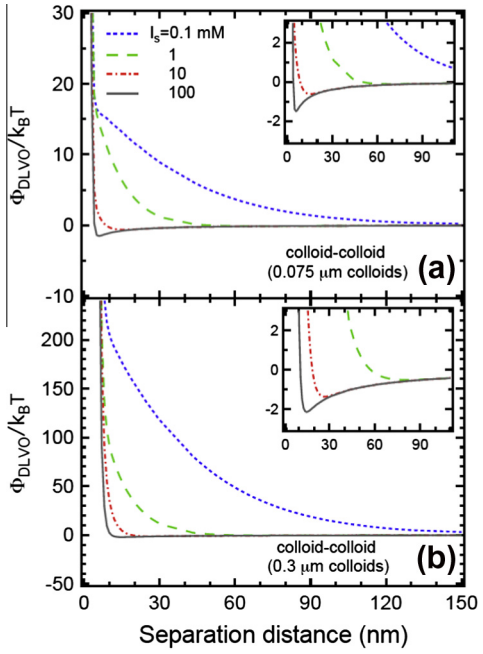

Fig. 9. Predicted colloid–colloid (sphere–sphere) Φ_{DLVO} energy interactions for I_s = 0.1, 1, 10, 100 mM with: (a) green microspheres (d_p = 0.075 μm), and (b) red microspheres (d_p = 0.3 μm), as a function of separation distance.

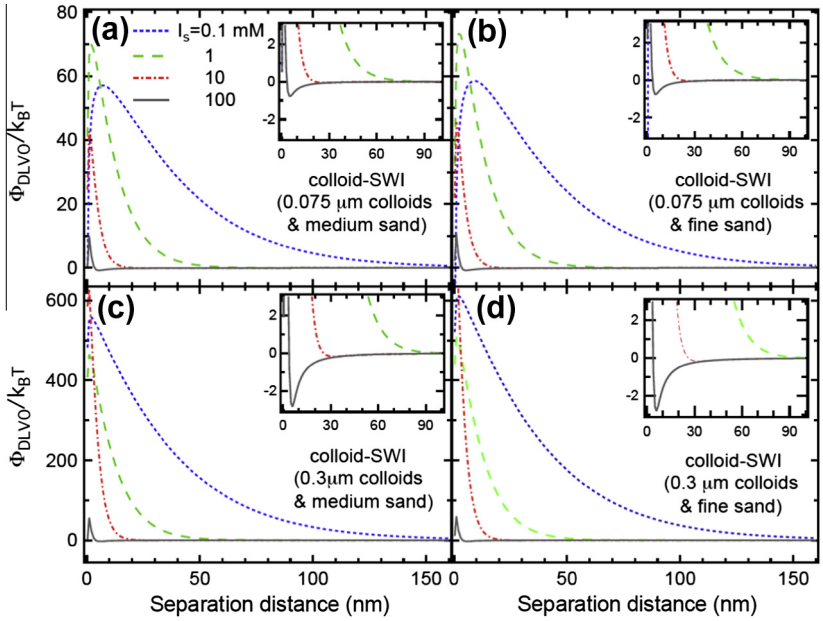

Fig. 10. Predicted colloid–SWI (sphere–plate) Φ_{DLVO} energy interactions for I_s = 0.1, 1, 10, 100 mM with: (a) green microspheres (d_p = 0.075 μm) and medium sand, (b) green microspheres (d_p = 0.075 μm) and fine sand, (c) red microspheres (d_p = 0.3 μm) and medium sand, and (d) red microspheres (d_p = 0.3 μm) and fine sand, as a function of separation distance.

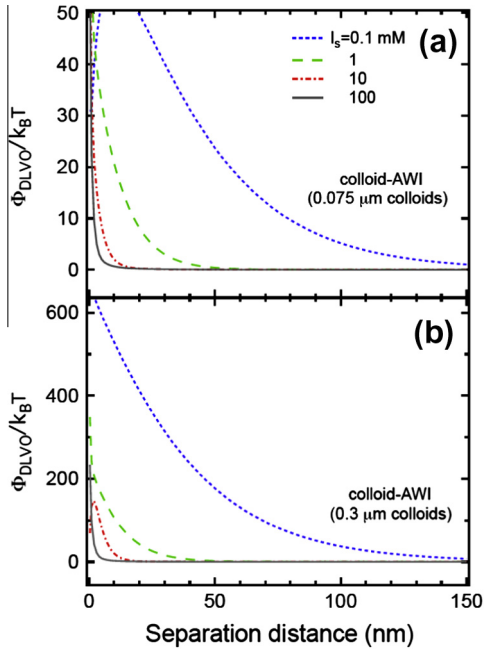

Fig. 11. Predicted colloid–AWI (sphere–plate) Φ_{DLVO} energy interactions for I_s = 0.1, 1, 10, 100 mM with: (a) green microspheres (d_p = 0.075 μm), and (b) red microspheres (d_p = 0.3 μm), as a function of separation distance.

The inclusion of the Born repulsion eliminated the attractive Φ_{min1}. It is evident from Fig. 9 that the colloid–colloid repulsion forces were dominant. Furthermore, based on the calculated Φ_{min2} values, the red microspheres possessed higher Φ_{min2} depth than the green microspheres, and thus the red microspheres were expected to coagulate easier. Nevertheless, no apparent coagulation was observed in neither of the two colloid suspensions. Fig. 10 presents colloid–SWI DLVO calculations, which show the presence of a significant energy barrier to attachment in the Φ_{min1} (of several 100 k_BT for the red microspheres and of several 10 k_BT for the green microspheres), and a shallow Φ_{min2} at greater distance from the SWI. It is evident from Table 3 that the depth of the Φ_{min2} increases with I_s ranging from 0.0002 k_BT at I_s = 0.1 mM to 0.7764 k_BT at I_s = 100 mM for the green microspheres (d_p = 0.075 μm) and from 0.0011 k_BT at I_s = 0.1 mM to 2.8434 k_BT at I_s = 100 mM for the red microspheres (d_p = 0.3 μm). This result is in agreement with the higher mass recovery values observed for the larger microspheres (see Table 2). Gravity has a negligible influence on Brownian particles. Therefore, deposition at Φ_{min2} occurs when hydrodynamic drag interaction energy and colloidal Brownian diffusion kinetic energy are balanced or exceeded by the attractive DLVO interaction energy. However, in most cases Φ_{min2} is smaller than 1.5 k_BT (the average kinetic energy of a colloid) therefore, physical and chemical surface heterogeneity could have a significant influence on DLVO energy profiles and colloid deposition at Φ_{min2} for different I_s [66]. Furthermore, the colloids may be held in Φ_{min2}; however, this cannot explain the observed grain size-dependent deposition. Therefore, another retention mechanism must also be involved.

Fig. 11 shows that the attachment of microspheres onto AWIs is not favorable. According to Schäfer et al. [15], the Hamaker constant for microspheres interacting with AWIs is negative (A_{1wa} = -1.05×10^{-20} J). Furthermore, given that the dielectric constant and the refractive index of air are equal to 1, the resulting van der Waals interaction energies are repulsive, and in turn the total interaction energies, Φ_{DLVO}, are repulsive for all separation distances. It should be noted that no Φ_{min2} exists for colloid–AWI interactions under the experimental conditions. Hence, permanent retention of dispersed colloids at AWIs cannot be expected under current experimental conditions (Φ_{min1} does not exist). However, Abdel-Fattah and El-Genk [67] reported that colloid–AWI interaction energies are not necessarily repulsive for all separation distances. Zevi et al. [24] observed that some colloids reside close to AWIs, at convergence or stagnation points. Furthermore, contrary to DLVO theory predictions, Wan and Wilson [12] reported that

Table 3
Estimated values of Φ_{min1}, Φ_{min2}, Φ_{max1}, and α_{th} for the green and red microspheres.

I_s (mM)	Interactions	Green microspheres (d_p = 0.075 μm)			α_{th} (−)	Red microspheres (d_p = 0.3 μm)			α_{th} (−)
		Φ_{min1} (k_BT)	Φ_{max1} (k_BT)	Φ_{min2} (k_BT)		Φ_{min1} (k_BT)	Φ_{max1} (k_BT)	Φ_{min2} (k_BT)	
0.1	Colloid–SWI (medium sand)	na	57.1	−0.0002	0.0001	na	558.3	−0.0011	0.0002
0.1	Colloid–SWI (fine sand)	−22.1	58.5	−0.0003	0.0001	na	611.8	−0.0010	0.0002
0.1	Colloid–colloid	na	na	−0.0115	na	na	na	−0.1015	na
0.1	Colloid–AWI	na	55.7	na	na	na	na	na	na
1	Colloid–SWI (medium sand)	na	70.0	−0.0040	0.0001	na	464.5	−0.0150	0.0011
1	Colloid–SWI (fine sand)	na	73.3	−0.0039	0.0000	na	510.2	−0.0146	0.0011
1	Colloid–colloid	na	na	−0.1080	na	na	na	−0.5141	na
1	Colloid–AWI	na	na	na	na	na	na	na	na
10	Colloid–SWI (medium sand)	na	42.7	−0.0595	0.0160	na	630.0	−0.1827	0.0527
10	Colloid–SWI (fine sand)	na	45.6	−0.0576	0.0098	na	na	−0.1776	na
10	Colloid–colloid	na	na	−0.6136	na	na	na	−1.3659	na
10	Colloid–AWI	na	na	na	na	na	146.6	na	na
100	Colloid–SWI (medium sand)	na	9.9	−0.7764	0.3293	na	55.9	−2.8434	0.8971
100	Colloid–SWI (fine sand)	na	10.7	−0.7639	0.3235	na	59.9	−2.8202	0.8690
100	Colloid–colloid	na	na	−1.5128	na	na	na	−2.1462	na
100	Colloid–AWI	na	na	na	na	na	na	na	na

polystyrene latex colloids attach strongly onto AWIs. This phenomenon may be explained by the existence of additional non-DLVO forces, i.e., hydrophobic forces, which operate over a longer range and are much stronger than the van der Waals and double layer forces [68,69].

Fig. 12 presents the experimental efficiencies, α_{exp}, as predicted by Eq. (6), and the theoretical collision efficiencies, α_{th}, as predicted by the Maxwell approximation (Eq. (17)), for colloid–SWI interactions, as a function of I_s for red microspheres (d_p = 0.3 μm), and green microspheres (d_p = 0.075 μm) in columns packed with medium sand. Both α_{exp} and α_{th} were shown to increase with increasing I_s. Discrepancies between α_{exp} and α_{th} within 1–1.5 orders of magnitude have also been reported in the literature by other investigators [29,45]. Note that the α_{th} calculations presented here assume that the sand and colloid surfaces are uniformly charged. However, it is highly probable that both the sand grains and the microspheres exhibit some surface charge heterogeneity [70]. The presence of hetero-domains of attractive surface charges is known to enhance colloid retention in the presence of energy barriers [71].

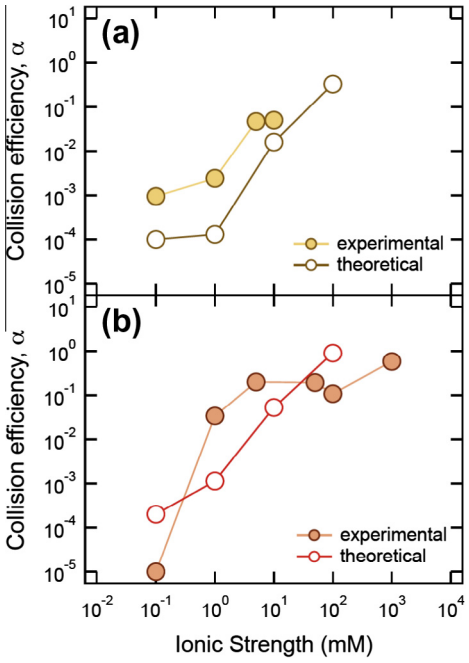

Fig. 12. Experimental (filled symbols) and theoretical (open symbols) collision efficiencies in unsaturated columns packed with medium sand as a function of ionic strength for: (a) green microspheres (d_p = 0.075 μm), and (b) red microspheres (d_p = 0.3 μm).

5. Summary

Numerous column experiments were carried out in order to investigate the effects of ionic strength and sand grain size on colloid transport and retention in unsaturated columns packed with quartz sand. The results of this study showed that larger microspheres (d_p = 2.1 μm) were retained slightly more than the conservative tracer and smaller microspheres (d_p = 0.3, and 0.075 μm) in deionized distilled water, possibly due to straining. Moreover, microsphere attachment was higher onto medium than fine sand, and for most of the cases examined, early breakthrough (velocity enhancement) of the microspheres was observed. The mass recovery of the microspheres was shown to significantly decrease with increasing ionic strength. More favorable attachment conditions existed for the red microspheres (d_p = 0.3 μm) than the green microspheres (d_p = 0.075 μm). Both α_{exp} and α_{th} increased with increasing ionic strength. Discrepancies between the estimated values of α_{exp} and α_{th} could be attributed to surface charge heterogeneities of the sand grains and/or microspheres. The results from this study suggest that the combined effect of ionic strength, sand grain size, colloid size, and degree of saturation play a significant role on breakthrough concentrations. Moreover, DLVO interaction energy calculations demonstrated that partitioning of colloids to the solid–water and air–water interfaces was insignificant across the range of the ionic strengths considered in this study. However, significant colloid retention occurred in the column, even under substantial energy barriers. Also, both the experimental collision efficiency and the theoretical collision efficiency increased with increasing ionic strength. Discrepancies between the estimated values of the experimental collision efficiency and the theoretical collision efficiency could be attributed to surface charge heterogeneities of the sand grains and/or microspheres.

Acknowledgments

This research has been co-financed by the European Union (European Social Fund-ESF) and Greek National Funds through the Operational program "Education and Lifelong Learning" under the action Aristeia I (Code No. 1185). This is collaborative work between members of the BioMet Network.

References

[1] A. Abdel-Salam, C.V. Chrysikopoulos, Analysis of a model for contaminant transport in fractured media in the presence of colloids, Adv. Water Resour. 17 (5) (1994) 283–296, http://dx.doi.org/10.1016/0309-1708(94)90032-9.

[2] Y. Sim, C.V. Chrysikopoulos, Three-dimensional analytical models for virus transport in saturated porous media, Transp. Porous Media 30 (1) (1998) 87–112, http://dx.doi.org/10.1023/A:1006596412177.

[3] C.V. Chrysikopoulos, S.C. James, Transport of neutrally buoyant and dense variably sized colloids in a two-dimensional fracture with anisotropic aperture, Transp. Porous Media 51 (2003) 191–210, http://dx.doi.org/10.1023/A:1021952226861.

[4] Y. Chu, Y. Jin, T. Baumann, M.V. Yates, Effect of soil properties on saturated and unsaturated virus transport through columns, J. Environ. Qual. 32 (2003) 2017–2025.

[5] R. Anders, C.V. Chrysikopoulos, Virus fate and transport during artificial recharge with recycled water, Water Resour. Res. 41 (10) (2005) W10415, http://dx.doi.org/10.1029/2004WR003419.

[6] J.M. Thomas, C.V. Chrysikopoulos, Experimental investigation of acoustically enhanced colloid transport in water-saturated packed columns, J. Colloid Interface Sci. 308 (2007) 200–207, http://dx.doi.org/10.1016/j.jcis.2006.12.062.

[7] C. Masciopinto, R. La Mantia, C.V. Chrysikopoulos, Fate and transport of pathogens in a fractured aquifer in the Salento area, Italy, Water Resour. Res. 44 (2008) W01404, http://dx.doi.org/10.1029/2006WR005643.

[8] V.I. Syngouna, C.V. Chrysikopoulos, Interaction between viruses and clays in static and dynamic batch systems, Environ. Sci. Technol. 44 (2010) 4539–4544, http://dx.doi.org/10.1021/es100107a.

[9] V.I. Syngouna, C.V. Chrysikopoulos, Cotransport of clay colloids and viruses in water saturated porous media, Colloids Surf. A: Physicochem. Eng. Aspects 416 (2013) 56–65, http://dx.doi.org/10.1016/j.colsurfa.2012.10.018.

[10] C.V. Chrysikopoulos, C. Masciopinto, R. La Mantia, I.D. Manariotis, Removal of biocolloids suspended in reclaimed wastewater by injection in a fractured aquifer model, Environ. Sci. Technol. 44 (3) (2010) 971–977.

[11] C.V. Chrysikopoulos, V.I. Syngouna, I.A. Vasiliadou, V.E. Katzourakis, Transport of Pseudomonas putida in a three-dimensional bench scale experimental aquifer, Transp. Porous Media 94 (2012) 617–642, http://dx.doi.org/10.1007/s11242-012-0015-z.

[12] J.M. Wan, J.L. Wilson, Visualization of the role of the gas–water interface on the fate and transport of colloids in porous media, Water Resour. Res. 30 (1994) 11–23.

[13] M.Y. Corapcioglu, H. Choi, Modeling colloid transport in unsaturated porous media and validation with laboratory column data, Water Resour. Res. 32 (1996) 3437–3449.

[14] J.M. Wan, T.K. Tokunaga, Film straining of colloids in unsaturated porous media: conceptual model and experimental testing, Environ. Sci. Technol. 31 (1997) 2413–2420.

[15] A. Schäfer, H. Harms, A.J.B. Zehnder, Bacterial accumulation at the air–water interface, Environ. Sci. Technol. 32 (1998) 3704–3712.

[16] Y. Chu, Y. Jin, M. Flury, M.V. Yates, Mechanisms of virus removal during transport in unsaturated porous media, Water Resour. Res. 37 (2) (2001) 253–263.

[17] G. Chen, M. Flury, Retention of mineral colloids in unsaturated porous media as related to their surface properties, Colloids Surf. A: Physicochem. Eng. Aspects 256 (2005) 207–216. (Corrections, Colloids Surf. A: Physicochem. Eng. Aspects 289 (2006) 254-255; Colloids Surf. A: Physicochem. Eng. Aspects, 396 (2012) 352–353).

[18] S. Torkzaban, S.A. Bradford, M.Th. van Genuchten, S.L. Walker, Colloid transport in unsaturated porous media: the role of water content and ionic strength on particle straining, J. Contam. Hydrol. 96 (2008) 113–127.

[19] G. Chen, S.L. Walker, Fecal indicator bacteria transport and deposition in saturated and unsaturated porous media, Environ. Sci. Technol. 46 (2012) 8782–8790.

[20] Y. Sim, C.V. Chrysikopoulos, Analytical models for virus adsorption and inactivation in unsaturated porous media, Colloids Surf. Physicochem. Eng. Aspects 155 (1999) 189–197, http://dx.doi.org/10.1016/S0927-7757(99)00073-4.

[21] Y. Sim, C.V. Chrysikopoulos, Virus transport in unsaturated porous media, Water Resour. Res. 36 (2000) 173–179, http://dx.doi.org/10.1029/1999WR900302.

[22] R. Anders, C.V. Chrysikopoulos, Transport of viruses through saturated and unsaturated columns packed with sand, Transp. Porous Media 76 (2009) 121–138, http://dx.doi.org/10.1007/s11242-008-9239-3.

[23] W. Zhang, V.L. Morales, M.E. Cakmak, A.E. Salvucci, L.D. Geohring, A.G. Hay, J.-Y. Parlange, T.S. Steenhuis, Colloid transport and retention in unsaturated porous media: effect of colloid input concentration, Environ. Sci. Technol. 44 (13) (2010) 4965–4972.

[24] Y. Zevi, A. Dathe, J.F. McCarthy, B.K. Richards, T.S. Steenhuis, Distribution of colloid particles onto interfaces in partially saturated sand, Environ. Sci. Technol. 39 (18) (2005) 7055–7064.

[25] B. Gao, J.E. Saiers, J. Ryan, Pore-scale mechanisms of colloid deposition and mobilization during steady and transient flow through unsaturated granular media, Water Resour. Res. 42 (1) (2006) W01410, http://dx.doi.org/10.1029/2005WR004233.

[26] S.A. Bradford, S. Torkzaban, Colloid transport and retention in unsaturated porous media: a review of interface-, collector-, and pore-scale processes and models, Vadose Zone J. 7 (2) (2008) 667–681.

[27] S. Veerapaneni, J.M. Wan, T.K. Tokunaga, Motion of particles in film flow, Environ. Sci. Technol. 34 (12) (2000) 2465–2471.

[28] C.A. Black (Ed.), Methods of Soil Analysis, Part 2, Chemical and Microbiological Properties, American Society of Agronomy, Madison, 1965.

[29] V.I. Syngouna, C.V. Chrysikopoulos, Transport of biocolloids in water saturated columns packed with sand: effect of grain size and pore water velocity, J. Contam. Hydrol. 126 (2011) 301–314, http://dx.doi.org/10.1016/j.jconhyd.2011.09.007.

[30] E.A. Stephan, G.G. Chase, A preliminary examination of zeta potential and deep bed filtration activity, Sep. Purif. Technol. 21 (2001) 219–226.

[31] A. Graciaa, G. Morel, P. Saulner, J. Lachaise, R.S. Schechter, The ζ-potential of gas bubbles, J. Colloid Interface Sci. 172 (1995) 131–136.

[32] C. Yang, T. Dabros, D.Q. Li, J. Czarnecki, J.H. Masliyah, Measurement of the zeta potential of gas bubbles in aqueous solutions by microelectrophoresis method, J. Colloid Interface Sci. 243 (2001) 128–135.

[33] C.V. Chrysikopoulos, Artificial tracers for geothermal reservoir studies, Environ. Geol. 22 (1993) 60–70.

[34] S.C. James, C.V. Chrysikopoulos, Monodisperse and polydisperse colloid transport in water-saturated fractures with various orientations: gravity effects, Adv. Water Resour. 34 (2011) 1249–1255, http://dx.doi.org/10.1016/j.advwatres.2011.06.001.

[35] K.M. Yao, M.T. Habibian, C.R. O'Melia, Water and waste water filtration: concepts and applications, Environ. Sci. Technol. 5 (11) (1971) 1105–1112.

[36] J.E. Saiers, J.J. Lenhart, Colloid mobilization and transport within unsaturated porous media under transient-flow conditions, Water Resour. Res. 39 (1) (2003) 1019, http://dx.doi.org/10.1029/2002WR001370.

[37] N. Tufenkji, M. Elimelech, Correlation equation for predicting single-collector efficiency in physicochemical filtration in saturated porous media, Environ. Sci. Technol. 38 (2004) 529–536.

[38] R. Kretzschmar, M. Borkovec, D. Grolimund, M. Elimelech, Mobile subsurface colloids and their role in contaminant transport, Adv. Agron. 65 (1999) 121–193.

[39] J.P. Loveland, J.N. Ryan, G.L. Amy, R.W. Harvey, The reversibility of virus attachment to mineral surfaces, Colloids Surf. A: Physicochem. Eng. Aspects 107 (1996) 205–221.

[40] D.L. Feke, N.D. Prabhu, J.A. Mann Jr., J.A. Mann III, A formation of the hort range repulsion between spherical colloidal particles, J. Phys. Chem. 88 (1984) 5735–5739.

[41] J.N. Ryan, P.M. Gschwend, Effect of ionic strength and flow rate on colloid release: Relating kinetics to intersurface potential, J. Colloid Interface Sci. 164 (1994) 21–34.

[42] J. Gregory, Approximate expressions for retarded van der Waals interaction, J. Colloid Interface Sci. 83 (1) (1981) 138–145.

[43] R. Hogg, T.W. Healy, D.W. Fuerstenau, Mutual coagulation of colloidal dispersions, Trans. Faraday Soc. 62 (1966) 1638–1651.

[44] E. Ruckenstein, D.C. Prieve, Adsorption and desorption of particles and their chromatographic separation, AIChE J. 22 (1976) 276–283.

[45] C. Shen, B. Li, Y. Huang, Y. Jin, Kinetics of coupled primary- and secondary-minimum deposition of colloids under unfavorable chemical conditions, Environ. Sci. Technol. 41 (2007) 6976–6982.

[46] F.J. Bueche, Introduction to physics for scientists and engineers, 2nd ed., McGraw-Hill, 1975, p. 870.

[47] S. Takahashi, A.R. Kovscek, Spontaneous countercurrent imbibition and forced displacement characteristics of low-permeability, siliceous shale rocks, J. Petrol. Sci. Eng. 71 (2010) 47–55.

[48] A. Santos, P. Bedrikovetsky, A stochastic model for particulate suspension flow in porous media, Transp. Porous Media 62 (2006) 23–53.

[49] W.P. Johnson, E. Pazmino, H. Ma, Direct observations of colloid retention in granular media in the presence of energy barriers, and implications for inferred mechanisms from indirect observations, Water Res. 44 (2010) 1158–1169.

[50] S.A. Bradford, M. Bettahar, Concentration dependent transport of colloids in saturated porous media, J. Contam. Hydrol. 82 (2006) 99–117.

[51] V.L. Morales, B. Gao, T.S. Steenhuis, Grain surface-roughness effects on colloidal retention in the vadose zone, Vadose Zone J. 8 (1) (2009) 11–20.

[52] G. Gargiulo, S.A. Bradford, J. Simunek, P. Ustohal, H. Vereecken, E. Klumpp, Bacteria transport and deposition under unsaturated conditions: the role of the matrix grain size and the bacteria surface protein, J. Contam. Hydrol. 92 (2007) 255–273.

[53] S. Torkzaban, S.A. Bradford, S.L. Walker, Resolving the coupled effects of hydrodynamics and DLVO forces on colloid attachment to porous media, Langmuir 23 (2007) 9652–9660.

[54] A.C. Alvarez, G. Hime, D. Marchesin, P.G. Bedrikovetsky, The inverse problem of determining the filtration function and permeability reduction in flow of water with particles in porous media, Transp. Porous Media 70 (2007) 43–62.

[55] C.Y. Shen, Y.F. Huang, B.G. Li, Y. Jin, Effects of solution chemistry on straining of colloids in porous media under unfavorable conditions, Water Resour. Res. 44 (5) (2008) W05419, http://dx.doi.org/10.1029/2007WR006580.

[56] X.Q. Li, C.L. Lin, J.D. Miller, W.P. Johnson, Role of grain-to-grain contacts on profiles of retained colloids in porous media in the presence of an energy barrier to deposition, Environ. Sci. Technol. 40 (12) (2006) 3769–3774.

[57] A.L. Mills, J.S. Herman, G.M. Hornberger, T.H. De Jesús, Effect of solution ionic strength and iron coatings on minerals grains on the sorption of bacterial cells to quartz sand, Appl. Environ. Microbiol. 60 (1994) 3300–3306.
[58] D.G. Jewett, T.A. Hilbert, B.E. Logan, R.G. Arnold, R.C. Bales, Bacterial transport in laboratory columns and filters: influence of ionic strength and pH on collision efficiency, Water Res. 29 (1995) 1673–1680.
[59] W.P. Johnson, B.E. Logan, Enhanced transport of bacteria in porous media by sediment-phase and aqueous-phase natural organic matter, Water Res. 30 (1996) 923–931.
[60] Y. Jin, M.V. Yates, S.S. Thompson, W.A. Jury, Sorption of viruses during flow through saturated sand columns, Environ. Sci. Technol. 31 (1997) 548–555.
[61] M.W. Hahn, D. Abadzic, C.R. O'Melia, Aquasols: on the role of secondary minima, Environ. Sci. Technol. 38 (2004) 5915–5924.
[62] S.A. Bradford, S. Torkzaban, S.L. Walker, Coupling of physical and chemical mechanisms of colloid straining in saturated porous media, Water Res. 41 (2007) 3012–3024.
[63] M. Tong, W.P. Johnson, Excess colloid retention in porous media as a function of colloid size, fluid velocity, and grain angularity, Environ. Sci. Technol. 40 (2006) 7725–7731.
[64] M. Tong, W.P. Johnson, Colloid population heterogeneity drives hyperexponential deviation from classic filtration theory, Environ. Sci. Technol. 41 (2007) 493–499.
[65] X. Li, T.D. Scheibe, W.P. Johnson, Apparent decreases in colloid deposition rate coefficient with distance of transport under unfavorable deposition conditions: a general phenomenon, Environ. Sci. Technol. 38 (2004) 5616–5625.
[66] S.A. Bradford, S. Torkzaban, Colloid interaction energies for physically and chemically heterogeneous porous media, Langmuir 29 (2013) 3668–3676.
[67] A.I. Abdel-Fattah, M.S. El-Genk, Sorption of hydrophobic microspheres onto a stagnant air/water interface, J. Colloid Interface Sci. 202 (1998) 417–429.
[68] J.N. Israelachvili, Intermolecular and Surface Forces, 2nd ed., Academic Press, London, 1992.
[69] C.V. Chrysikopoulos, V.I. Syngouna, Attachment of bacteriophages MS2 and ΦX174 onto kaolinite and montmorillonite: extended DLVO interactions, Colloids Surfaces B: Biointerfaces 92 (2012) 74–83, http://dx.doi.org/10.1016/j.colsurfb.2011.11.028.
[70] S.L. Walker, J.A. Redman, M. Elimelech, Role of cell surface lipopolysaccharides (LPS) in Escherichia coli K12 adhesion and transport, Langmuir 20 (2004) 7736–7746.
[71] M. Auset, A.A. Keller, Pore-scale visualization of colloid straining and filtration in saturated porous media using micromodels, Water Resour. Res. 42 (2006) W12S02, http://dx.doi.org/10.1029/2005WR004639.